RUSSIAN JOURNAL OF EARTH SCIENCES
vol. 16, 3, 2016, doi: 10.2205/2016ES000573

Orientation distribution function of biotite platelets based on optical, thin sections and μ-CT image analysis in an Outokumpu (Finland) biotite gneiss: Comparison with neutron diffraction texture analysis

O. G. Duliu[1,2], *T. I. Ivankina*[2], *E. Herman*[3], *C. Richman*[4], *I. Tiseanu*[5]

[1]University of Bucharest, Faculty of Physics, Magurele, Ilfov, Romania

[2]Frank Laboratory of Neutron Physics, Joint Institute for Nuclear Research, Dubna, Moscow Region, Russia

[3]University of Bucharest, Doctoral School of Physics, Magurele, Ilfov, Romania

[4]Geological Institute of Romania, National Museum of Geology, Bucharest, Romania

[5]National Institute for Laser, Plasma and Radiation Physics, Magurele, Ilfov, Romania

Abstract. The results of the neutron diffraction investigation were compared with similar results obtained by analysing more μ-CT, high resolution photographic and thin section images of a cylindrical sample of the textured Outokumpu (Finland) biotite gneiss. All data were interpreted by means of corresponding orientation distribution function (ODF). Both Rayleigh R test of uniformity and Rao's U test for homogeneity of the corresponding ODF confirmed the existence of a real anisotropic distribution of mineralogical phases within investigated specimens. Together with the neutron diffraction pole figures, ODF, unambiguously proved the existence of a lattice as well as of the shape preferred orientations of the mineralogical components of the complex Outokumpu gneiss.

This is the e-book version of the article, published in Russian Journal of Earth Sciences (doi:10.2205/2016ES000573). It is generated from the original source file using LaTeX's **ebook.cls** class.

Introduction

Finland occupies a large part of the Baltic (Fenoscandian) Shield, mainly consisting of Archaean and Proterozoic gneisses and greenstone, multiply contorted during the past tectonic activity. Here, in the South-Eastern part the Outokumpu mining district lies a sulphide deposit rich in the economic grades Co, Ni, Cu, Zn and Ag. Since 1910, about 50 Mt of sulphide ore with an average content of 0.2% Co, 2.8% Cu and 1% Zn were extracted and subsequently processed. The Outokumpu sulphide deposit presents an unusual diverse lithological association with a medium to high metamorphic grade, whose origin was not yet completely elucidated. Previous seismic studies have evidenced the presence of a strong reflectivity level coincident with the sulphide rich section [*Heinonen et al.,* 2011]. In view of this, between 2004 and 2005, at Outokumpu, a deep research borehole (62^o 43' 4" N, 29^o 3' 43" E) (Figure 1) was drilled which finally reached a depth of 2516 m [*Kukkonen*, 2011].

The sulphide rich level which lays at a depth of 1850 m belongs to the lower gneiss series and consists of an alternation of biotite gneiss and pegmatitic granite with

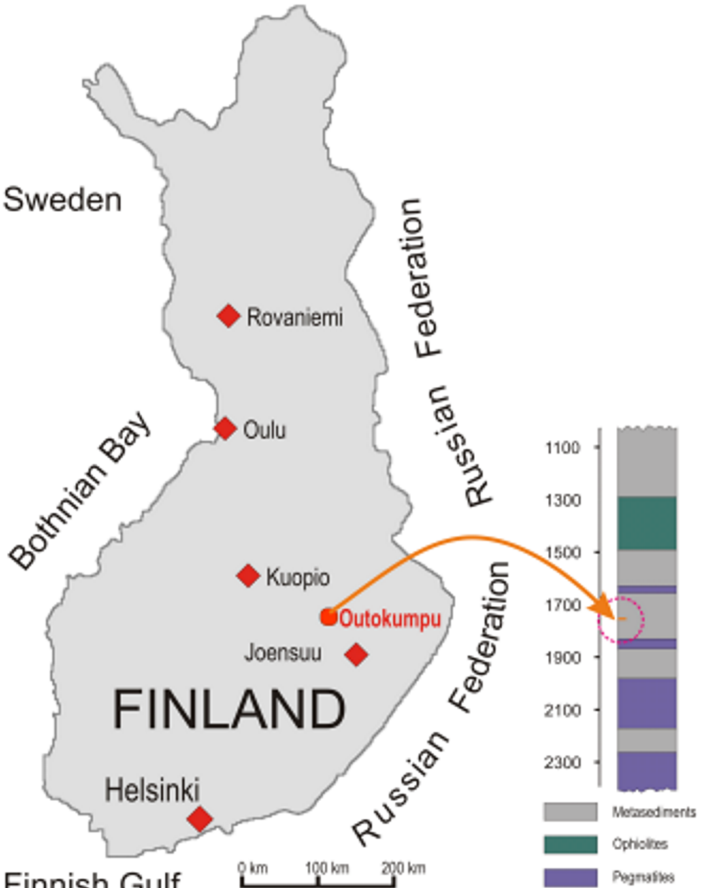

Figure 1. The Outokumpu Deep Drilling Project location showing the position of the Outokumpu 1844 sample location with respect to the neighbouring main lithological units.

thin intercalation of amplibolites. The bedded biotite-gneiss presents a variable mineralogical composition, mainly consisting of muscovite or biotite mica, quartz and feldspars with small amounts of andalusite, garnets, sillimanite, kyanite or staurolite [*Västi*, 2011]. As a result, in the biotite-gneiss layers, the biotite platelets lay almost horizontally. Moreover, laboratory determination of the P- and S-wave velocities indicated not only a strong anisotropy of the biotite-gneiss rocks but also the presence of microcracks, not completely closed. These peculiarities were interpreted as one of the main cause of the marked reflection of the seismic waves previously evidenced by high resolution seismic reflection [*Kern and Mengel,* 2011]. The anisotropy of the seismic waves is controlled by a complex of factors concerning both physical environment such as local pressure and temperature and essential rock properties such as mineral composition, Crystallographic Preferred Orientation (CPO), Shape Preferred Orientation (SPO), degree of crystallinity, foliation, lineation, etc.

The anisotropy of the rock properties can be investigated either at the level of the crystalline lattice or at the level of the composing mineral. In the first case the neutron diffraction gave the best results [*Ivankina et al.,* 2005; *Lokajicek et al.,* 2014; *Barreiro et*

al., 2015] while in the second case the image analysis of thin section or μ-computed tomography (μ-CT) are preferred [*Jerram and Higgins,* 2007]. The information provided by these methods are rather complementary as the neutron diffraction data refer to the mineral lattices CPO while the optical methods evidence only the external shape of the composing crystals SPO [*Song et al.,* 2001; *Plotkina et al.,* 2006; *Baker et al.,* 2012]. However, there is no detailed investigation and documentation on how CPO and SPO are related to one another. Consequently, their concurrent use could better characterize the rock structure, the best results being obtained in the case of strongly deformed metamorphic rocks such as biotite gneiss.

Materials and Methods

We have used for analyses a biotite-gneiss disk of about 3 cm thickness extracted from the Outokumpu core i.e. sample OKU 1844 (depth of 1844.5 m). From this segment, few sections were extracted by a diamond saw to get final samples for neutron diffraction and μ-CT investigations. For neutron diffraction we have selected a cylindrical fragment with a diameter of 3 cm and a thickness of 3 cm, while for μ-CT we have selected a

significantly smaller sample, also of a cylindrical shape, but with a diameter of only 1.5 cm (Figure 2c). In samples, the foliation was found to be oriented normal to the core (borehole) axis (Z axis). As 2400 dpi scanned images (Figure 2f1, f2) and thin sections photographs (Figure 3) showed, the sample has a strongly foliate granoblastic structure consisting of assemblages of biotite, quartz and plagioclase. The thin sections are in general oriented parallel to foliation (XY-plane).

Neutron diffraction measurements for texture analysis were done by means of the time-of-flight (TOF) texture diffractometer SKAT at the Frank Laboratory of Neutron Physics at JINR (Dubna, Russia) [*Ullemeyer et al.,* 1998; *Keppler et al.,*2014]. Its resolution allowed sufficient number of not overlapped pole figures to be extracted from the diffraction spectra by simple integration of the peak intensity after background subtraction. From the experimental pole figures the ODFs were determined and, by applying the WIMF method and the corresponding software Beartex, it was possible to recalculate the pole figures for the predominant mineral phases [*Ivankina and Matthies,* 2015].

All 3D μ-CT scan were performed by using a homemade computed tomography provided with a microfocus X-ray tube working at 135 kV and 0.1 mA fil-

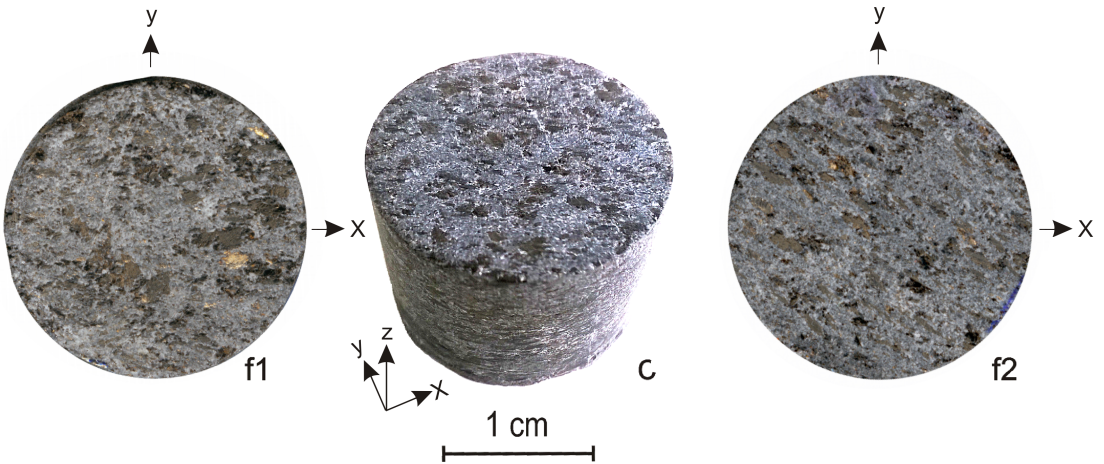

Figure 2. A photographic image of the Outokumpu sample (c) as well as two 2400 dpi scanned images of the opposed faces of the same sample (fl and f2).

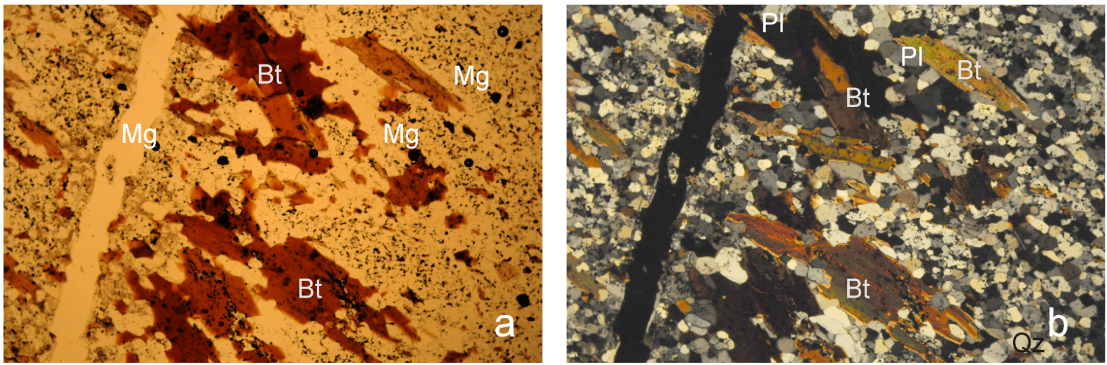

$N_{||}$, 10x / 0.25 Pol N_{+}, 10x / 0.25 Pol

Figure 3. Two representative images illustrating the same thin sections segment of the Outokumpu 1844 biotite gneiss obtained in parallel (a) and cross (b) Nicols. Besides plagioclase feldspar (Pl), quartz (Qz) and magnetite (Mg), both images illustrate the presence of strongly deformed, almost acicular biotite crystals (Bi).

tered by a 0.1 mm Cu filter. The instrument spatial resolution, better than 50 μm allows representing the material grains whose size is larger than this threshold [*Tiseanu et al.,* 2011, 2013].

Photographic images of the opposed surfaces of sample were realized by a 2400 dpi scanner so grains with a minimum size of 50 μm could be well observed.

The polarized light thin sections images were obtained by means of a Nikon Eclipse LV100Pol polarized light microscope, permitting to identify the major minerals. A total of $2x15$ different microscopic images (parallel and crossed Nicols), similar to those reproduced in Figure 3 were recorded and then analyzed.

In order to calculate for each category of images, i.e. μ-CT, scanned or polarized microscopy the corresponding ODF, were have used the Image SXM software [*Image SXM,* 2016; https://www.liverpool.ac.uk/ sdb/ ImageSXM/] by following few steps:

- Image Pre-processing – Scaling the image; Improving the contrast, luminosity and colors; Applying of background corrections and noise removal;
- Segmentation – identification of image segments that represent relevant objects; Separation of different materials using various graphic filters to se-

lect the chosen material;

- Analysis – approximation, by ellipses, of the previously selected objects by segmentation;
- Calculation, for each category of objects, of the corresponding ODF and displaying it by means of rose diagrams. During calculation, we have used some GIMP filters. Once calculated, each ODF was represented as rose diagram, by means of the PAST; software [*Hammer et al.,* 2001].

As ODF are represented in polar coordinates, we have used the Rayleigh R test of uniformity which gives the probability that the data are not unidirectional as well as the Rao's U test for homogeneity of angular data [*Jmmalamadaka et al.,*2001] to check at which extent the corresponding ODF point toward an anisotropic minerals orientation. The PAST software [*Hammer et al.,* 2001] was used for these calculations too. Since both pole figures and rose diagrams have the same reference frame, this enables correlation between CPO and SPO of mineral constituents.

Results and Discussion

Preliminary XRF data regarding the major, rock forming elements (*Tugulan et al.,* unpublished results), sho-

wed for the investigated sample a rather felsic origin with the following composition (in wt %): SiO_2 - 65.66, TiO_2 - 0.60, Al_2O_3 - 11.73, FeO - 7.25, MnO - 0.08, MgO - 3.63, CaO - 2.56, Na_2O - 3.74, K_2O - 2.75.

A careful analysis of the photographic images of the gneiss sample (Figure 2c) evidenced a foliar structure normal to the sample longitudinal axis, coincident within few degrees with the core axis. At the same time, the high resolution photographic images of the superior as well as the inferior polished surfaces of the sample (Figure 2f1, f2) show a shape preferred orientation (SPO) of the dark biotite crystals as well as of the other features. Hence, in an orthogonal frame, whose Z axis coincides with the sample vertical axis both photographic images correspond to the lineation XY plane. These observations are confirmed by the images reproduced in Figure 3 which illustrate one fragment the thin sections parallel to the sample upper surface and photographed under polarized light.

In this regard, Figure 4 displays the μ-CT images of three mutually perpendicular sections throughout the Outokumpu gneiss as well as the corresponding ODF. The first section lies parallel to the sample surface, while the other two illustrates a longitudinal and a coronal section respectively. It is worth mentioning that the

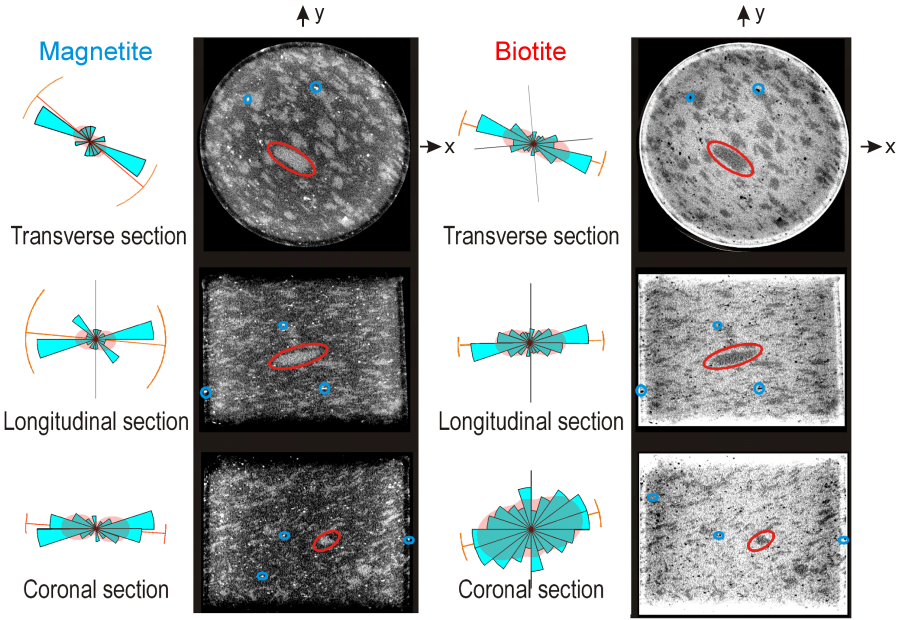

Figure 4. Three μ-CT images of the biotite gneiss sample OKU 1844 corresponding to three mutually perpendicular sections, according to the coordinate system illustrated in Figure 2. For a better illustration, both negative and positive CT images are reproduced. The rose diagrams illustrate the SPO of biotite and magnetite grains. The average value $\pm$ standard deviation of the corresponding ODF are graphically represented here and in Figure 6 and Figure 7 by red lines.

longitudinal section corresponds to the longest biotite axis while the coronal section, perpendicular to the longitudinal one, illustrates the biotite platelet shorter axis. Biotite long shape axes are generally oblique to foliation (horizontal direction in Figure 4) by 10 degrees.

The calculated principal pole figures of the sample Outocumpu 1844 based on neutron diffraction measurements are shown in Figure 5. The biotite (001) pole figure is unimodal, the degree of preferred orientation is large with a maximum of 9.08 m.r.d.; the intensity maximum parallels the foliation normal. The poles to the (100) + (010)-planes are concentrated on a great circle within the foliation plane. The textures of quartz and plagioclase are also well pronounced, but are much weaker than those of biotite. It is worthy to note, that the pole figures of biotite are in general symmetrically disposed to foliation and lineation with a small rotation of about 10 degrees towards to the lineation direction X (Figure 5, inset).

Starting from the photographic and μ-CT images of the Outokumpu 1844 gneiss (Figure 3 and Figure 4) as well as from neutron diffraction data (Figure 5), the Image SXM software was used to calculate the corresponding ODFs and to display them as rose diagrams [*Heillbronner and Barrett,* 2014] and to recalculate pole

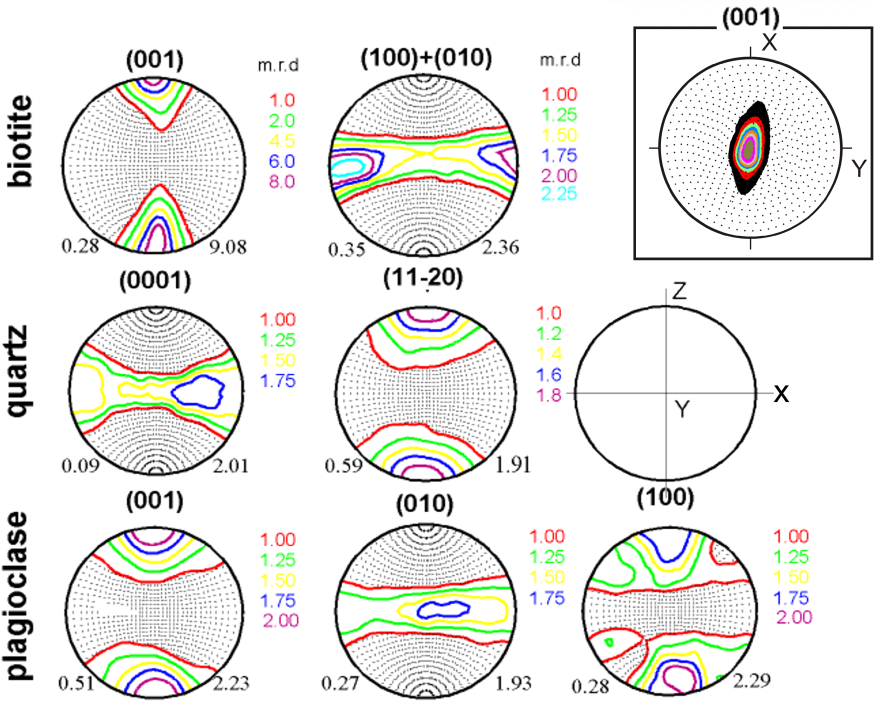

Figure 5. Complete quantitative texture analysis of the biotite gneiss sample OKU 1844 performed by neutron diffraction. Principal pole figures of biotite, quartz and plagioclase (equal area projection, upper hemisphere) are illustrated. Pole density contours are in multiple of a random distribution (m.r.d). In the top right hand corner there is inset showing biotite (001) pole distributions in the rotated stereogram.

figures respectively [*Ivankina and Matthies,* 2015].

Therefore, the Figure 5, Figure 6, and Figure 7 illustrate the most important outcomes of the OKU 1844 biotite gneiss ODFs investigation, i.e. both foliation and lineation, as well as mineral CPOs and SPOs.

Indeed, Figure 5 which contains the biotite, quartz and plagioclase pole figures, as obtained by neutron diffraction, illustrates the presence of a single maximum normal to the foliation, much sharper in the case of biotite. Biotite, due to its six-sided monoclinic unit cells, tends to form elongated parallelogram or hexagonal platelets with sides of different lengths. Obviously, differently oriented biotite platelets (ellipsoidal grains) possess hard-wired crystal lattice [*Matthies,* 2012]. This peculiarity is proved by the fact that biotite long axes on rose diagram (Figure 4) and orientation of biotite (001) poles on pole (Figure 5) are rotated to the lineation direction X by 10 degrees.

The other major minerals such as quartz or plagioclase whose crystals present a more regular shape are less aligned and consequently, their pole figures show corresponding weaker orientations (see Figure 5). Moreover, strong correlations between quartz and plagioclase CPOs and SPOs are not apparent.

The same remark is sustained by the ODF repre-

sented by the rose diagrams reproduced in Figure 6 and Figure 7 and obtained by the analyses of the photographic as well as CT. In all cases, the corresponding ODF point towards a significant anisotropy of orientations corresponding to constituent mineral phases, differentiated by colour on photographic images or by X-ray attenuation on CT images. In the case of CT images, the mineral phases with higher densities appear in lighter hues on the negative images. In this way, it was possible to evidence not only the gneiss foliation, but the existing lineation, better observed within foliation plane. This peculiarity is well documented by the ODF functions of corresponding μ-CT images displayed in the Figure 4. Here, for a better illustration, both negative and positive CT images were reproduced.

It should be remarked that in the cases of CT (Figure 4), photographic (Figure 6) as well as thin sections (Figure 7) ODF, Rayleigh R test of uniformity and Rao's U test for homogeneity, point towards a real anisotropic distribution of mineral phases within investigated specimens of gneiss at $p < 0.01$ (the probability of the null hypothesis: all crystal are uniformly distributed).

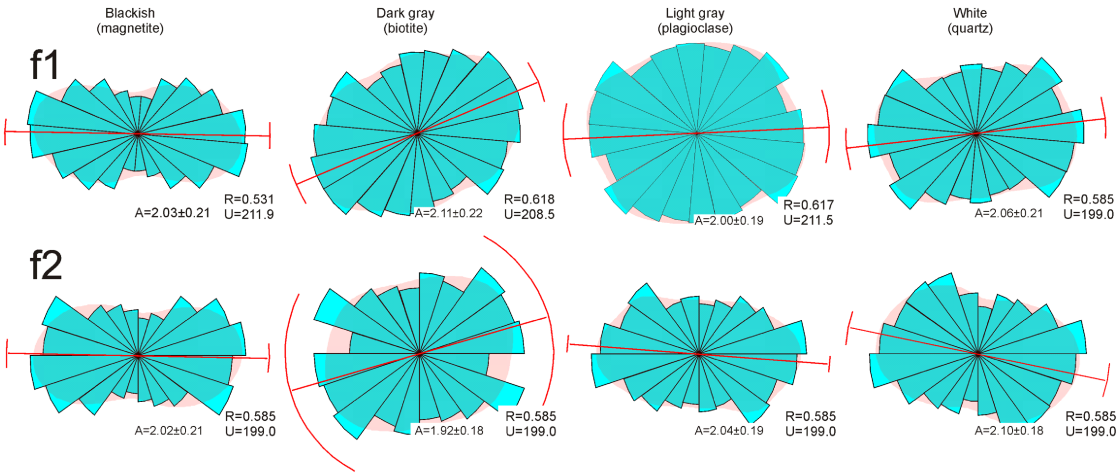

Figure 6. Rose diagrams illustrating the ODF of different mineral fractions as resulted from the analysis of Figure 2 images. Black corresponds to biotite platelets, while dark grey, light grey and white could be attributed to plagioclase and quartz. In all cases the anisotropy parameter has a value of about 2, while both Rayleigh R and Rao's U tests point towards with a 99% probability of a non-uniform, anisotropic distribution of different minerals that compose samples.

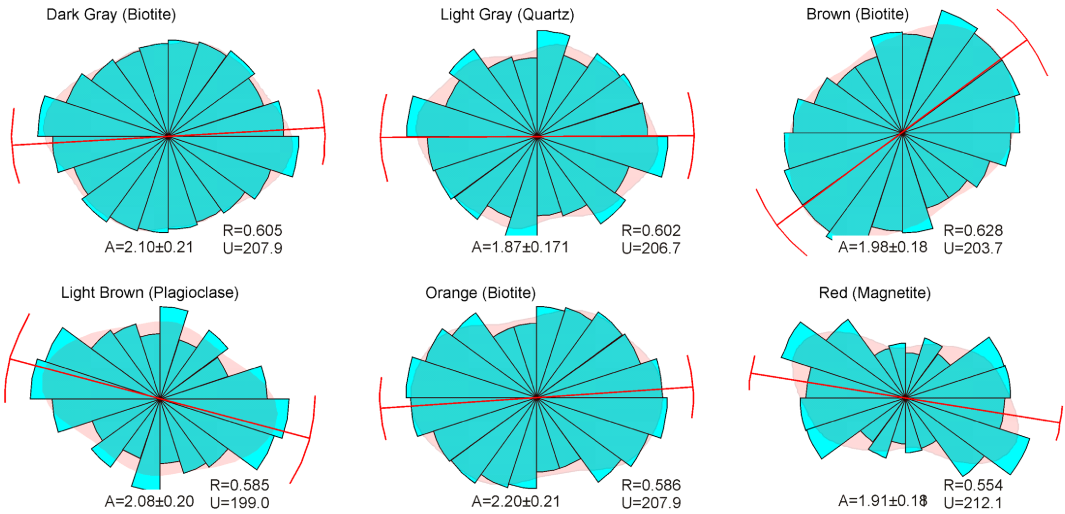

Figure 7. Rose diagrams illustrating the ODF of different mineral fractions based on the analysis of photographic images reproduced in Figure 3. The numerical values of the Rayleigh R and Rao's U parameter are reproduced too, which sustain the hypothesis of a non-uniform, anisotropic distribution of mineral components.

Concluding Remarks

The final purpose of this study was to characterize the existing non-uniformity in a complex textured rocks. This task supposed two stages: i to choose the most appropriate technique able to reveal the CPOs and SPOs of rock-forming minerals; and (ii) to find the best suited mathematical method able to analyze and compare the obtained information.

In our case, i.e. the Outokumpu 1844 biotite gneiss, the best results were get by combining neutron diffraction with image analysis (thin section, polished surfaces and CT images), the final results being in all cases the corresponding ODF. This allowed to represent the CPO as well as the SPO descriptor functions of the biotite gneiss sample, allowing to evidence both lineation and foliation, common traits of high grad metamorphic rocks. Although addressed to different characteristics of complex rocks, both neutron diffraction and image analysis, the last one regardless its source (optic, polarized light, CT), give the mutual complementary information concerning the rock structure.

In all cases, the ODF showed to be the best descriptor as it was able to unambiguously prove and characterize the lattice and shape preferred orientations of

complex rocks similar to the Outokumpu 1844 biotite gneiss.

Acknowledgments. This work was partially done within the cooperation protocol No. 4428-4-2015/2017 between the University of Bucharest and the Joint Institute for Nuclear Physics in Dubna, Russian Federation. The authors thank H. Kern (Kiel, Germany) for providing study rock sample from the Outokumpu borehole.

References

Baker, D.R. (2012), An introduction to the application of Xray microtomography to the three-dimensional study of igneous rocks, *Lithos, 148*, 262–276, doi:10.1016/j.lithos.2012.06.008

Barreiro, J. G., H.-R. Wenk, S. Vogel (2015), Texture and elastic anisotropy of a mylonitic anorthosite from the Morin Shear Zone (Quebec, Canada), *Journal of Structural Geology, 71*, 100–111, doi:10.1016/j.jsg.2014.07.021

Hammer, O, D. A. T. Harper, P. D. Ryan (2001), Paleontological statitics software package for education and data analysis, *Paleontologia Electronica, 4*, 9, (http://palaeo-electronica.org/2001_1/past/issue1_01.htm)

Heillbronner, R., S. Barrett (2014), Segmentation by Poin Operation, Image Analysis in Earth Sciences; *Microstructures and Textures of Earth Materials* p. 77–94, Springer, Berlin. (ISBN: 978-3-642-10343-8)

Heinonen, S., I. T. Kukkonen, P. J. Heikkinen, R. Douglas, D. S.

Schmitt (2011), High Resolution Reflection Seismics Integrated With Deep Drill Hole Data in *Outokumpu, Outokumpu Deep Drilling Project 2003–2010*, (Ed. I.T. Kukkonen) p. 105118, Geological Survey of Finland, Helsinki. (http://tupa.gtk.fi/julkaisu/specialpaper/sp_051.pdf)

Ivankina, T. I., H. Kern, A. N. Nikitin (2005), Directional dependence of P- and S-wave propagation and polarization in foliated rocks from the Kola superdeep well: Evidence from laboratory measurements and calculations based on TOF neutron diffraction, *Tectonophysics, 407*, 25–42, doi:10.1016/j.tecto.2005.05.029

Ivankina, T. I., S. Matthies (2015), On the development of quantitative texture analysis and its application in solving problems of Earth Sciences, *Physics of Particles and Nuclei, 46*, 366–423, doi:10.1134/S1063779615030077

Jammalamadaka, S., A. Sen Gupta (2011), Topics in Circular Statistics, *Multivariate Analysis, Vol. 5* (Ed. M. M. Rao) p. 330, World Scientific, Singapore. (ISBN 9810237782)

Jerram, D.A., M.D. Higgins (2007), 3D analysis of rock textures: quantifying igneous microstructures, *Elements*, 3, 239–245, (http://www.geo.mtu.edu/EHaz/ConvergentPlatesClass/dougal jerram/Jerram_Higgins_Elements2007.pdf)

Keppler, R., K. Ullemeyer, J. H. Behrman, M. Stipp (2014), Potential of full pattern fit methods for the texture analysis of geological materials: implications from texture measurements at the recently upgraded neutron time of flight diffractometer SKAT, *Journal of Applied Crystallography, 47*, 1520–1534,

doi:10.1107/S1600576714015830

Kern, H., K. Mengel, (2011), High Resolution Reflection Seismics Integrated With Deep Drill Hole Data in *Outokumpu, Outokumpu Deep Drilling Project 2003–2010*, (Ed. I.T. Kukkonen) p. 105–118, Geological Survey of Finland, Helsinki. (http://tupa.gtk.fi/julkaisu/specialpaper/sp_051.pdf)

Kukkonen, I.T. (2011), Outokumpu Deep Drilling Project, *Outokumpu Deep Drilling Project 2003-2010*, (Ed. I.T. Kukkonen) p. 1252, Geological Survey of Finland, Helsinki. (http://tupa.gtk.fi/julkaisu/specialpaper/sp_051.pdf)

Lokajicek, T, H. Kern, T. Svitek, T. I. Ivankina (2014), 3D velocity distribution of P- and S-waves in a biotite gneiss, measured in oil as the pressure medium: Comparison with velocity velocity measurements in a multi-anvil pressure apparatus and with texture-based calculated data, *Physics of Earth and Planet Interior, 241*, 1–15, doi:10.1016/j.pepi.2014.04.002

Matthies, S. (2012), GEO-MIX-SELF calculations of the elastic properties of a textured graphite sample at different hydrostatic pressure, *Journal of Applied Crystalography, 45*, 1–16, doi:10.1107/S002188981104338X

Plotkina, Yu. V., E. B. Salnikova, A. B. Kotlov, M. D. Tolkachev, M. R. Pavlov (2006), Computer microtomography of zircon: A new approach to the selection of targets for U-Pb geochronologic studies, *Petrology, 14*, 201–208, doi:10.1134/S0869591106020044

Song, S.-R., K. W. Joned, B. W. Lindquist, B. A. Dowd, D. L. Sahagian (2001), Synchrotron X-ray computed microtomography: studies on vesiculated basaltic rocks, *Bulletin of Volcanology,*

63, 252–263, doi:10.1007/s004450100141

Tiseanu, I., T. Craciunescu, B. Pegourier, M. Hans, C. Ruset, M. Mayer, C. Dobre, A. Sima (2011), Advanced X-ray imaging of metal-coated/impregnated plasma-facing composite materials, *Physica Scripta, 145*, id 014073, doi:10.1088/0031-8949/2011/T145/014073

Tiseanu, I., L. Zani, T. Craciunescu, F. Cotorobai, C. Dobre, A. Sima (2013), Characterization of superconducting wires and cables by X-ray micro-tomography, *Fusion Engineering and Design, 88*, 1613–1618, doi:10.1016/j.fusengdes.2013.03.065

Ullemeyer, K., P. Spalthoff, J. Heintz, N.N. Iaskov, A.N. Nikitin, K. Weber (1998), The SKAT texture diffractometer at the pulsed reactor IBR-2 at Dubna: experimental layout and first measurements, *Nuclear Instruments and Methods in Physics Research A, 412*, 80–88, doi:10.1016/S0168-9002(98) 00340-4

Vasti, K. (2011), Petrology of the drill hole R2500 at Outokumpu, eastern Finland – the deepest drill hole ever drilled in Finland, *Outokumpu Deep Drilling Project 2003–2010*, (Ed. I.T. Kukkonen) p. 1–252, Geological Survey of Finland, Helsinki. (http://tupa.gtk.fi/julkaisu/specialpaper/sp_051.pdf) doi:10.1016/j.lithos.2012.06.008